5

Numerical Modeling of Photonic Crystal Circuits Using Fourier Series Expansion Method Based on Floquet-Modes

Koki Watanabe[1] and Kiyotoshi Yasumoto[2]
[1]*Fukuoka Institute of Technology*
[2]*Professor Emeritus of Kyushu University*
Japan

1. Introduction

Microwave waveguides are usually composed of metals and dielectrics. The high contrast of their electromagnetic parameters benefits that the electromagnetic energy is strongly confined near the waveguiding structures and propagates along them. However, metal waveguides in millimeter and sub-millimeter wave regions are often suffered from large attenuations because the conductor loss of metal rapidly increases with the operating frequency. This is a reason why optical fiber, which is a waveguide for much higher frequency ranges, is composed of dielectrics only and avoids the use of metals. Then, the dielectric waveguides are widely investigated in millimeter and sub-millimeter wave regions to get rid of the conductor loss. They are typically composed of the core and the surrounding cladding. The refractive index of the core is some larger than that of the cladding. The fields propagating along a dielectric waveguide are not totally confined as with a metallic waveguide, and they are composed of the guided modes and the radiation modes. These modes are coupled to each other when the waveguide structure is not uniform along the wave propagation. Then the bending loss tends to be large in the dielectric waveguides. This is an obstacle to realize integrated circuits. The photonic crystal waveguide attracts attention as a waveguiding structure that resolves this problem.

The photonic crystals are periodic dielectric structures that are designed to reject the propagation of electromagnetic waves at certain wavelength range. Local collapses of the periodicity supply significant advantages for field confinement, wave guiding, and directing radiation. Especially, defects introduced into the photonic crystals compose electromagnetic wave devices such as cavities, waveguides, splitter, coupler, etc. and they constitute photonic crystal circuits. The photonic crystals are composed of dielectrics only and the conductor loss is negligible in many cases. Also, the electromagnetic fields are strongly confined around the defects because any energy cannot escape through the surrounding photonic crystal. These features provide a significant progress towards reducing the size of electromagnetic wave circuits. The electromagnetic wave propagation along the photonic crystal circuits has been simulated using various numerical methods such as the beam propagation method(Koshiba et al., 2000), the finite difference time domain (FDTD) method(Taflove, 1995), and the plane wave expansion method(Benisty, 1996). These methods require adequate treatments of terminating conditions for the waves at the output ends of the circuits. However, the structure of photonic

crystal waveguide is nonuniform along the wave propagation, and the Floquet-mode analysis is necessary to decompose the fields in input/output waveguides into the forward and the backward propagating components. The Floquet-modes are the eigenmodes propagating in a structure periodic along the wave propagation.

The guided Floquet-modes propagating in straight photonic crystal waveguides are sometimes analyzed by FDTD method with the help of the super-cell method(Sakoda et al., 1997) or Prony's method(Naka & Ikuno, 2002). However, since the computation errors are comparatively easy to accumulate in periodic structures, FDTD method seems to require special techniques in accurate calculations. The structure is fully periodic in the propagation direction, and several papers(Jia & Yasumoto, 2006; Tanaka et al., 1994; Yasumoto et al., 2004) introduce therefore the generalized Fourier series to expand the electromagnetic fields. Maxwell's equations and the constitutive relations yield a coupled ordinary differential-equation set in terms of the generalized Fourier coefficients. Then, the dispersion equation is derived based on the scattering-matrix (S-matrix) propagation algorithm for multilayer structures(Li, 1996a). The derived dispersion equation is written by a complex function with a complex argument and the zeros correspond to the propagation constants of the eigenmodes. These approaches make us possible to obtain the guided Floquet-modes in very high accuracy, but they are not applicable to obtain the evanescent ones.

Consideration of the evanescent modes is possible by the Fourier series expansion method (FSEM), which was originally developed to analyze the discontinuities in dielectric waveguides(Hosono et al., 1982; Yamakita et al., 1993; Yasumoto et al., 1999). This method introduces an artificial periodicity in the transverse direction and expresses the electromagnetic fields in the Fourier series expansion. The waveguiding structure is sliced into segments uniform in the propagation direction, and Maxwell's equations and the constitutive relations in each segment yield a coupled ordinary differential-equation set for the Fourier coefficients of field components. Since the coefficients of the coupled differential-equation set are constant, the general solution for each segment can be obtained by an eigenvalue/eigenvector calculation. The field coefficients are matched at the boundary between the segments, and we can obtain the propagation characteristics for composite structure. Miyamoto et al.(Miyamoto et al., 2003) calculated the Floquet-modes propagating in grating waveguides using FSEM. The Floquet-modes are obtained by the eigenvalue analysis of the transfer matrix for one periodicity cell in the propagation direction. Their formulation was applied to the Floquet-mode analyses of photonic crystal waveguides(Li & Ho, 2003; Watanabe & Yasumoto, 2009; Yasumoto & Toyama, 2001; Yasumoto & Watanabe, 2008a).

To show the basic idea of FSEM based on Floquet-mode concept, this chapter considers the two-dimensional electromagnetic fields propagating in electromagnetic wave circuits formed by defects in a photonic crystal, which consists of periodic array of rectangular cylinders. All dielectrics under consideration are linear, isotropic, lossless media, and the permeability of free space is assumed. The structure and fields are uniform in the y-direction, and two fundamental polarization are expressed by the transverse electric (TE) and the transverse magnetic (TM) polarizations, in which the electric and the magnetic fields are respectively perpendicular to the y-axis. We consider only time-harmonic fields assuming a time-dependence in $e^{-i\omega t}$, and the fields are represented by complex vectors depending only on the space variables x and z.

2. Floquet-Mode Analysis of Straight Photonic Crystal Waveguides

In this section, we consider the fields propagating in a straight photonic crystal waveguides schematically shown in Fig. 1(a). The photonic crystal consists of rectangular cylinders located parallel in rectangular lattice characterized by the periods d_x and d_z in the x- and z-directions, respectively. Each cylinder has common dimensions a_x and a_z along the x- and z-directions, and infinitely long in the y-direction. The permittivity of rectangular cylinders is denoted by ε_c and that of the surrounding media is denoted by ε_s. Choosing the appropriate parameters, the cylinder array forms the photonic crystal, which rejects the wave propagation. The waveguide is formed by straight line defects in the photonic crystal, and we assume that the fields are well confined in the x-direction.
Let $\varepsilon(x,z)$ be the permittivity distribution. Then Maxwell's curl equations and the constitutive relations yield the following relations:

$$\frac{\partial}{\partial z} H_x(x,z) - \frac{\partial}{\partial x} H_z(x,z) = -i\omega\varepsilon(x,z) E_y(x,z) \tag{1}$$

$$\frac{\partial}{\partial z} E_y(x,z) = -i\omega\mu_0 H_x(x,z) \tag{2}$$

$$\frac{\partial}{\partial x} E_y(x,z) = i\omega\mu_0 H_z(x,z) \tag{3}$$

$$\frac{\partial}{\partial z} E_x(x,z) - \frac{\partial}{\partial x} E_z(x,z) = i\omega\mu_0 H_y(x,z) \tag{4}$$

$$\frac{\partial}{\partial z} H_y(x,z) = i\omega\varepsilon(x,z) E_x(x,z) \tag{5}$$

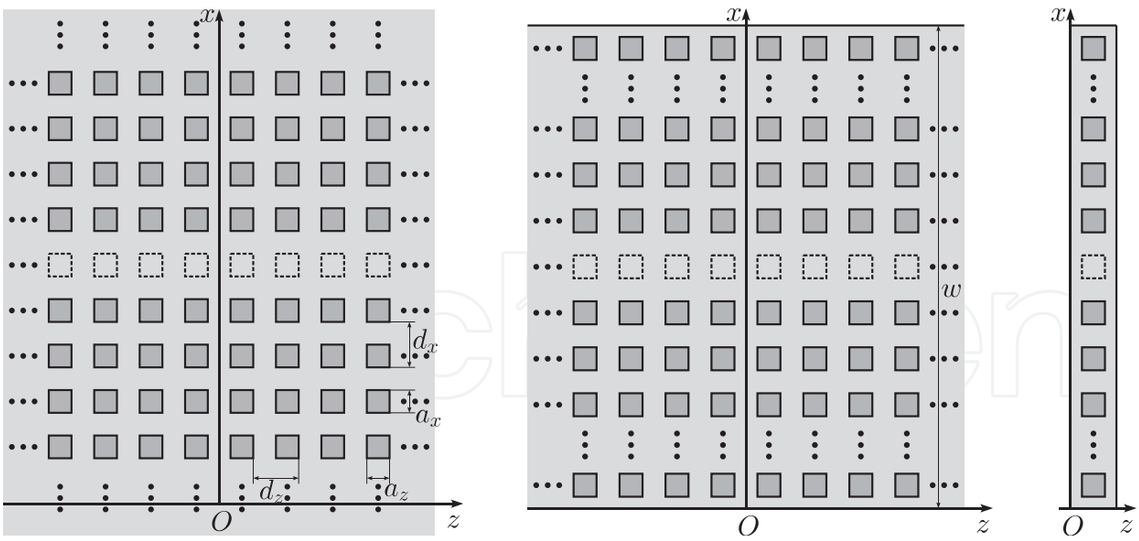

(a) (b) (c)

Fig. 1. Two-dimensional photonic crystal waveguide formed by rectangular cylinders, (a) original structure, (b) introduction of artificial boundaries with periodicity condition, and (c) periodicity cell for analysis.

$$\frac{\partial}{\partial x} H_y(x,z) = -i\omega\varepsilon(x,z)\, E_z(x,z). \tag{6}$$

Equations (1)–(3) correspond to the TE-polarization and Eqs. (4)–(6) correspond to the TM-polarization.
We introduce artificial boundaries at $x = 0$ and $x = w$, which are supposed to be sufficiently far from the line defect and not to make an unnecessary space near the boundaries (see Fig. 1(b)). The original electromagnetic fields in $0 < x < w$ are then approximated by periodic functions with the period w and expressed in the Fourier series expansions. For example, the y-component of electric field is approximately expressed as

$$E_y(x,z) = \sum_{n=-N}^{N} E_{y,n}(z)\, e^{i n k_w x} \tag{7}$$

where N denotes the truncation order and $k_w = 2\pi/w$. The Fourier coefficients $\{E_{y,n}(z)\}_{n=-N}^{N}$ are functions of z, and the field profile can be derived by calculating the z-dependence of the coefficients. To treat the coefficients systematically, we introduce $(2N+1)\times 1$ column matrices; for example, the coefficients of $E_y(x,z)$ are expressed by a column matrix $\boldsymbol{e}_y(z)$ that is defined by

$$\boldsymbol{e}_y(z) = \begin{pmatrix} E_{y,-N}(z) & \cdots & E_{y,N}(z) \end{pmatrix}^t \tag{8}$$

where the superscript t denotes the transpose matrix. Then, replacing all the field components by the Fourier series expansions and using the orthogonal property of the Fourier basis, Eqs. (1)–(6) yield the following relations:

$$\frac{d}{dz}\boldsymbol{h}_x(z) - i\boldsymbol{X}\boldsymbol{h}_z(z) = -i\omega[\![\varepsilon]\!]\boldsymbol{e}_y(z) \tag{9}$$

$$\frac{d}{dz}\boldsymbol{e}_y(z) = -i\omega\mu_0\boldsymbol{h}_x(z) \tag{10}$$

$$\boldsymbol{X}\boldsymbol{e}_y(z) = \omega\mu_0\boldsymbol{h}_z(z) \tag{11}$$

$$\frac{d}{dz}\boldsymbol{e}_x(z) - i\boldsymbol{X}\boldsymbol{e}_z(z) = i\omega\mu_0\boldsymbol{h}_y(z) \tag{12}$$

$$\frac{d}{dz}\boldsymbol{h}_y(z) = i\omega\left[\!\!\left[\frac{1}{\varepsilon}\right]\!\!\right]^{-1}\boldsymbol{e}_x(z) \tag{13}$$

$$\boldsymbol{X}\boldsymbol{h}_y(z) = -\omega[\![\varepsilon]\!]\boldsymbol{e}_z(z) \tag{14}$$

where $\boldsymbol{X}$ denotes a diagonal matrix whose diagonal elements are $\{nk_w\}_{n=-N}^{N}$, and $[\![\varepsilon]\!]$ and $[\![1/\varepsilon]\!]$ are square Toeplitz matrices whose (n,m)-entries are given by the $(n-m)$th-order Fourier coefficients of $\varepsilon(x,z)$ and $1/\varepsilon(x,z)$, respectively. The expressions on the right-hand sides in Eqs. (9), (13), and (14) are obtained by taking into account Li's Fourier factorization rules(Li, 1996b).
The entries of $[\![\varepsilon]\!]$ and $[\![1/\varepsilon]\!]$ are functions of z. Here, we slice the analysis region into segments uniform in the z-direction, and denote the regions $l\,d_z + (d_z - a_z)/2 < z < l\,d_z + (d_z + a_z)/2$ and $l\,d_z - (d_z - a_z)/2 < z < l\,d_z + (d_z - a_z)/2$ for any integer l as segments g and s, respectively. The permittivity distribution in the segment g is also denoted by $\varepsilon_g(x)$ though that in the segment s is a constant value ε_s. The Toeplitz matrices $[\![\varepsilon]\!]$ and $[\![1/\varepsilon]\!]$ are constant matrices $[\![\varepsilon_g]\!]$ and $[\![1/\varepsilon_g]\!]$ in the segment g, and constant diagonal matrices $\varepsilon_s\boldsymbol{I}$ and $(1/\varepsilon_s)\boldsymbol{I}$ in the segment s, where $\boldsymbol{I}$ denotes the identity matrix.

Then the general solutions to the coupled differential-equation set (9)–(14) in the segments $r = g,s$ are obtained by the eigenvalue/eigenvector calculations in the following forms:

$$\begin{pmatrix} \boldsymbol{e}_y(z) \\ \boldsymbol{h}_x(z) \end{pmatrix} = \boldsymbol{Q}_r^{(e)} \begin{pmatrix} \boldsymbol{a}_r^{(e,+)}(z) \\ \boldsymbol{a}_r^{(e,-)}(z) \end{pmatrix} \tag{15}$$

$$\begin{pmatrix} \boldsymbol{h}_y(z) \\ \boldsymbol{e}_x(z) \end{pmatrix} = \boldsymbol{Q}_r^{(h)} \begin{pmatrix} \boldsymbol{a}_r^{(h,+)}(z) \\ \boldsymbol{a}_r^{(h,-)}(z) \end{pmatrix} \tag{16}$$

with

$$\boldsymbol{Q}_g^{(e)} = \begin{pmatrix} \boldsymbol{P}_g^{(e)} & \boldsymbol{P}_g^{(e)} \\ -\frac{1}{\omega\mu_0}\boldsymbol{P}_g^{(e)}\boldsymbol{Z}_g^{(e)} & \frac{1}{\omega\mu_0}\boldsymbol{P}_g^{(e)}\boldsymbol{Z}_g^{(e)} \end{pmatrix} \tag{17}$$

$$\boldsymbol{Q}_g^{(h)} = \begin{pmatrix} \boldsymbol{P}_g^{(h)} & \boldsymbol{P}_g^{(h)} \\ \frac{1}{\omega}\left[\!\left[\frac{1}{\varepsilon_g}\right]\!\right]\boldsymbol{P}_g^{(h)}\boldsymbol{Z}_g^{(h)} & -\frac{1}{\omega}\left[\!\left[\frac{1}{\varepsilon_g}\right]\!\right]\boldsymbol{P}_g^{(h)}\boldsymbol{Z}_g^{(h)} \end{pmatrix} \tag{18}$$

$$\boldsymbol{Q}_s^{(e)} = \begin{pmatrix} \boldsymbol{I} & \boldsymbol{I} \\ -\frac{1}{\omega\mu_0}\boldsymbol{Z}_s^{(e)} & \frac{1}{\omega\mu_0}\boldsymbol{Z}_s^{(e)} \end{pmatrix} \tag{19}$$

$$\boldsymbol{Q}_s^{(h)} = \begin{pmatrix} \boldsymbol{I} & \boldsymbol{I} \\ \frac{1}{\omega\varepsilon_s}\boldsymbol{Z}_s^{(h)} & -\frac{1}{\omega\varepsilon_s}\boldsymbol{Z}_s^{(h)} \end{pmatrix} \tag{20}$$

$$\boldsymbol{P}_g^{(p)} = \begin{pmatrix} \boldsymbol{p}_{g,1}^{(p)} & \cdots & \boldsymbol{p}_{g,2N+1}^{(p)} \end{pmatrix} \tag{21}$$

$$\left(\boldsymbol{Z}_r^{(p)}\right)_{n,m} = \delta_{n,m}\,\gamma_{r,n}^{(p)} \tag{22}$$

for $p = e,h$, where ${\gamma_{g,n}^{(p)}}^2$ and $\boldsymbol{p}_{g,n}^{(p)}$ denote respectively the nth-eigenvalues and the associated eigenvectors of the matrices $\boldsymbol{C}_g^{(e)} = \omega^2\mu_0[\![\varepsilon_g]\!] - \boldsymbol{X}^2$ for the TE-polarization and $\boldsymbol{C}_g^{(h)} = [\![1/\varepsilon_g]\!]^{-1}\left(\omega^2\mu_0\boldsymbol{I} - \boldsymbol{X}[\![\varepsilon_g]\!]^{-1}\boldsymbol{X}\right)$ for the TM-polarization, and $\gamma_{s,n}^{(p)} = \sqrt{\omega^2\varepsilon_s\mu_0 - (\boldsymbol{X})_{n,n}{}^2}$. The column matrices $\boldsymbol{a}_r^{(p,+)}(z)$ and $\boldsymbol{a}_r^{(p,-)}(z)$ give the amplitudes of the local normal modes of the segment $r = g,s$ propagating in the $+z$- and $-z$-directions, respectively, and the relation between the modal amplitudes at $z = z'$ and $z = z''$ is given as

$$\begin{pmatrix} \boldsymbol{a}_r^{(p,+)}(z') \\ \boldsymbol{a}_r^{(p,-)}(z') \end{pmatrix} = \boldsymbol{U}_r^{(p)}(z'-z'') \begin{pmatrix} \boldsymbol{a}_r^{(p,+)}(z'') \\ \boldsymbol{a}_r^{(p,-)}(z'') \end{pmatrix} \tag{23}$$

with

$$\boldsymbol{U}_r^{(p)}(z) = \begin{pmatrix} \boldsymbol{V}_r^{(p)}(z) & \boldsymbol{0} \\ \boldsymbol{0} & \boldsymbol{V}_r^{(p)}(-z) \end{pmatrix} \tag{24}$$

$$\left(\boldsymbol{V}_r^{(p)}(z)\right)_{n,m} = \delta_{n,m}\,e^{i\gamma_{r,n}^{(p)}z}. \tag{25}$$

The structure under consideration is periodic in the z-direction, and the Floquet theorem asserts that analysis region can be reduced in one periodicity cell to characterize the propagation

property. Here, the periodicity cell is taken to be the region $0 < z < d_z$ (see Fig. 1(c)). The fields in segments g and s should be matched at the boundaries $z = (d_z \pm a_z)/2$ by the boundary conditions, which are given by continuing the coefficient column matrices for the tangential field components. Using Eqs. (15), (16), and (23), the relation between the modal amplitudes $\boldsymbol{a}_s^{(p,\pm)}(0)$ and $\boldsymbol{a}_s^{(p,\pm)}(d_z)$ are derived as

$$\begin{pmatrix} \boldsymbol{a}_s^{(p,+)}(d_z) \\ \boldsymbol{a}_s^{(p,-)}(d_z) \end{pmatrix} = \boldsymbol{F}^{(p)} \begin{pmatrix} \boldsymbol{a}_s^{(p,+)}(0) \\ \boldsymbol{a}_s^{(p,-)}(0) \end{pmatrix} \tag{26}$$

where the transfer matrix for the periodicity cell $\boldsymbol{F}^{(p)}$ is given by

$$\boldsymbol{F}^{(p)} = \boldsymbol{U}_s^{(p)} \left(\frac{d_z - a_z}{2} \right) \boldsymbol{Q}_s^{(p)^{-1}} \boldsymbol{Q}_g^{(p)} \boldsymbol{U}_g^{(p)}(a_z) \boldsymbol{Q}_g^{(p)^{-1}} \boldsymbol{Q}_s^{(p)} \boldsymbol{U}_s^{(p)} \left(\frac{d_z - a_z}{2} \right). \tag{27}$$

The Floquet-modes propagating in the photonic crystal waveguides are obtained by the eigenvalue analysis of the transfer matrix $\boldsymbol{F}^{(p)}$. Let $\beta_n^{(p)}$ and $\boldsymbol{r}_n^{(p)}$ be the nth-eigenvalues and the associated eigenvectors of $\boldsymbol{F}^{(p)}$, respectively. We define a column matrix $\boldsymbol{b}^{(p)}(z)$ by

$$\boldsymbol{b}^{(p)}(z) = \boldsymbol{R}^{(p)^{-1}} \begin{pmatrix} \boldsymbol{a}_s^{(p,+)}(z) \\ \boldsymbol{a}_s^{(p,-)}(z) \end{pmatrix} \tag{28}$$

with

$$\boldsymbol{R}^{(p)} = \begin{pmatrix} \boldsymbol{r}_1^{(p)} & \cdots & \boldsymbol{r}_{4N+2}^{(p)} \end{pmatrix} \tag{29}$$

and denote the nth-component of $\boldsymbol{b}^{(p)}(z)$ by $b_n^{(p)}(z)$. Then, from Eqs. (26) and (28), we obtain a relation:

$$b_n^{(p)}(d_z) = \beta_n^{(p)} b_n^{(p)}(0). \tag{30}$$

This implies that $\{b_n(0)\}_{n=1}^{4N+2}$ gives the amplitudes of the Floquet-modes propagating in the photonic crystal waveguide at $z = 0$, and the propagation constants are calculated by

$$\eta_n^{(p)} = -i \frac{\mathrm{Ln}(\beta_n^{(p)})}{d_z} \tag{31}$$

where Ln denotes the principal natural logarithm function. Also, considering Eqs. (15), (16), and (28), the Fourier coefficients of the modal profile functions corresponding to the nth-order Floquet-modes at $z = 0$ are given by

$$\begin{pmatrix} \boldsymbol{e}_y(0) \\ \boldsymbol{h}_x(0) \end{pmatrix} = \boldsymbol{Q}_s^{(e)} \boldsymbol{r}_n^{(e)} \tag{32}$$

$$\begin{pmatrix} \boldsymbol{h}_y(0) \\ \boldsymbol{e}_x(0) \end{pmatrix} = \boldsymbol{Q}_s^{(h)} \boldsymbol{r}_n^{(h)} \tag{33}$$

where Eq. (32) is for the TE-polarization and Eq. (33) is for the TM-polarization.
The propagation direction of each Floquet-mode can be judged as follows:

- if $|\beta_n^{(p)}| < 1$, the corresponding mode is the evanescent one propagating in the $+z$-direction.
- if $|\beta_n^{(p)}| > 1$, the corresponding mode is the evanescent one propagating in the $-z$-direction.
- if $|\beta_n^{(p)}| = 1$, the corresponding mode is the guided one. When the modal power carried in the z-direction is positive (negative), the corresponding mode propagates in the $+z$ ($-z$)-direction.

The z-component of the Poynting vector is given by

$$\begin{aligned} s_z(x,z) &= E_x(x,z)\, H_y(x,z)^* - E_y(x,z)\, H_x(x,z)^* \\ &= \sum_{n=-N}^{N} \sum_{m=-N}^{N} \left(E_{x,n}(z)\, H_{y,m}(z)^* - E_{y,n}(z)\, H_{x,m}(z)^* \right) e^{i(n-m)k_g x} \end{aligned} \tag{34}$$

and, integrating $s_z(x,z)$ over $0 \le x \le w$, we may obtain the following expression:

$$\int_0^w s_z(x,z)\, dx = w \left(\boldsymbol{e}_x(z) \cdot \boldsymbol{h}_y(z)^* - \boldsymbol{e}_y(z) \cdot \boldsymbol{h}_x(z)^* \right). \tag{35}$$

Therefore, the time-averaging modal power carried in the z-direction is calculated by $-w\,\Re(\boldsymbol{e}_y(0) \cdot \boldsymbol{h}_x(0)^*)/2$ for the TE-polarization and $w\,\Re(\boldsymbol{e}_x(0) \cdot \boldsymbol{h}_y(0)^*)/2$ for the TM-polarization, where $\boldsymbol{e}_y(0)$, $\boldsymbol{h}_x(0)$, $\boldsymbol{h}_y(0)$, and $\boldsymbol{e}_x(0)$ are obtained by Eqs. (32) and (33). The order of $\boldsymbol{F}^{(p)}$ $(p = e,h)$ is $4N+2$, and the eigenvalues $\{\beta_n^{(p)}\}_{n=1}^{4N+2}$, the propagation coefficients $\{\eta_n^{(p)}\}_{n=1}^{4N+2}$, and the eigenvectors $\{\boldsymbol{r}_n^{(p)}\}_{n=1}^{4N+2}$ are here supposed to be arranged in such a way that $\{\beta_n^{(p)}\}_{n=1}^{2N+1}$, $\{\eta_n^{(p)}\}_{n=1}^{2N+1}$, and $\{\boldsymbol{r}_n^{(p)}\}_{n=1}^{2N+1}$ correspond to the Floquet-modes propagating in the $+z$-direction and that $\{\beta_n^{(p)}\}_{n=2N+2}^{4N+2}$, $\{\eta_n^{(p)}\}_{n=2N+2}^{4N+2}$, and $\{\boldsymbol{r}_n^{(p)}\}_{n=2N+2}^{4N+2}$ correspond to ones propagating in the $-z$-direction.

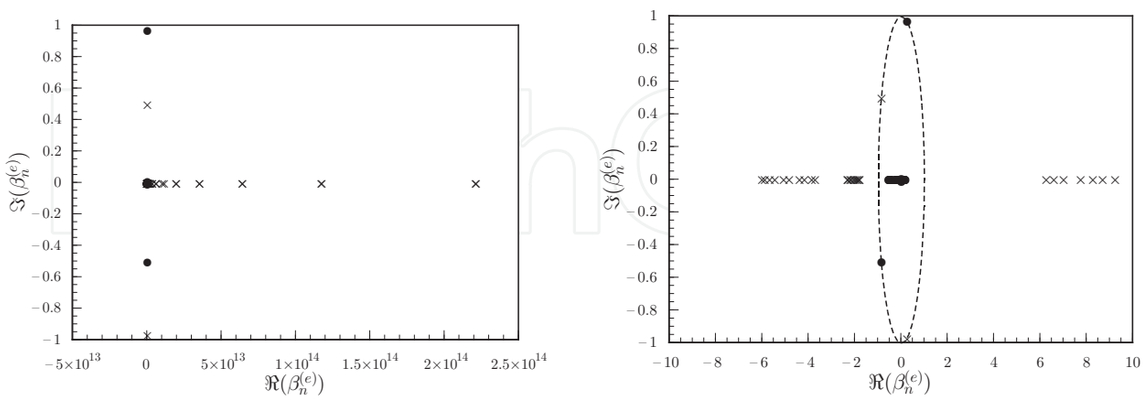

(a) (b)

Fig. 2. Distribution of the eigenvalues $\{\beta_n^{(e)}\}$ in the complex-plane, (a) whole view and (b) close view near the origin. (Reproduced from K. Watanabe and K. Yasumoto, *Progress In Electromagnetics Research*, PIER 92, 209–222, 2009, with courtesy of EMW Publishing.)

The eigenvalues $\{\beta_n^{(e)}\}$ calculated with $N = 60$ for the TE-polarization are plotted on the complex-plane in Fig. 2. The parameters of the photonic crystal are chosen as $\varepsilon_s = \varepsilon_0$, $\varepsilon_c = 12.25\,\varepsilon_0$, $d_x = d_z = 0.67\,\lambda_0$, and $a_x = a_z = \sqrt{0.41}\,d_x$. The rectangular cylinders are situated with the center at $x = (m - 1/2)\,d_x$ for positive integer m though one layer of cylinder array is removed at $x = 5.5\,d_x$ to form the waveguide structure, and $w = 11\,d_x$ is used for the periodic boundary condition. The photonic crystal waveguide with these parameters supports two guided modes. The dots and the crosses denote the eigenvalues correspond to the Floquet-mode propagating in the $+z$- and the $-z$-directions, respectively. Fig. 2(b) is a close view near the origin and the dashed curve denotes a circle with a unit radius. The values on the dashed curve correspond to the guided modes, and those corresponding to the forward and the backward propagating modes are respectively distributed inside and outside the circle. A whole view is given in Fig. 2(a) and shows that the spectral radius of the transfer matrix $\boldsymbol{F}^{(e)}$ (maximum absolute value of $\beta_n^{(e)}$) is about 2.2×10^{14}. This implies that the double precision computation leads to roundoff errors in the order of 10^{-2} and the obtained eigenvalues with $|\beta_n^{(e)}| \lesssim 10^{-2}$ may not be accurate. As a result, the calculation of the Floquet-modes propagating in the $-z$-direction are more accurate than ones propagating in the $+z$-direction, and the situation should be same for the TM-polarization.

Figure 3(a) shows the normalized propagation constants $\{\eta_n^{(e)}/k_d\}$ calculated from the eigenvalues plotted in Fig. 2, where $k_d = 2\pi/d_z$ denotes the inverse lattice constant in the z-direction. Jia and Yasumoto(Jia & Yasumoto, 2006) have calculated the normalized propagation constants of the guided Floquet-modes as 0.415946 for the even-mode and 0.219867 for the odd-mode. The normalized propagation constants of the guided Floquet-modes are plotted on the real axis in Fig. 3(a), and their values are ± 0.417 and ± 0.211. They are thought to be in a sufficiently good agreement with the reference values. If η is a propagation constant of Floquet-mode, $-\eta$ is also the propagation constant because of the structural symmetry. The

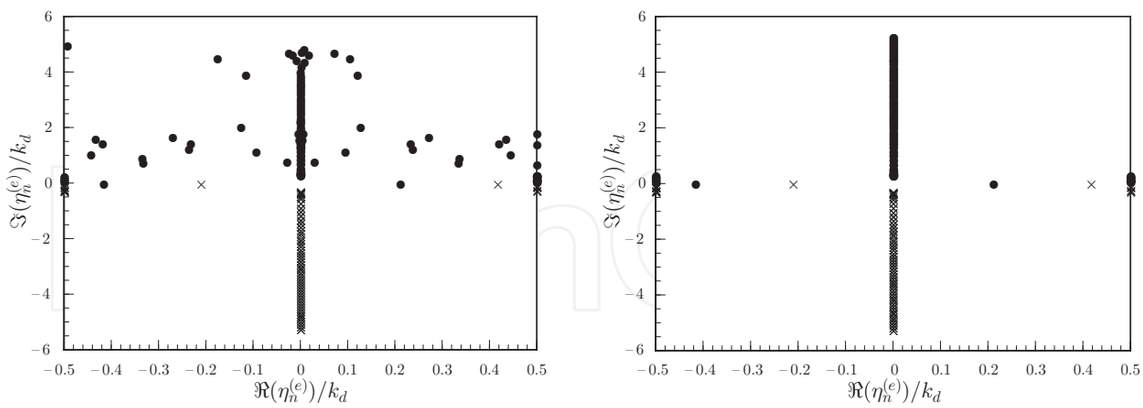

Fig. 3. Distribution of the normalized propagation constants $\{\eta_n^{(e)}/k_d\}$ with $k_d = 2\pi/d_z$ in the complex-plane, (a) direct results and (b) results with the use of the symmetric property. (Reproduced from K. Watanabe and K. Yasumoto, *Progress In Electromagnetics Research*, PIER 92, 209–222, 2009, with courtesy of EMW Publishing.)

distribution of $\{\eta_n^{(e)}\}$ should be therefore point symmetric to the origin. However, it is clearly observed in Fig. 3(a) that the symmetry for the obtained evanescent modes is broken due to the roundoff error, which is unnegligible for the propagation constants with large $\Im(\eta_n^{(e)})$.
Using the symmetric property, the accuracy of the Floquet-modes propagating in the $+z$-direction can be improved. Let $\boldsymbol{R}_1^{(p)}$ and $\boldsymbol{R}_2^{(p)}$ be $(2N+1)\times(2N+1)$ square matrices defined by

$$\begin{pmatrix}\boldsymbol{R}_1^{(p)}\\ \boldsymbol{R}_2^{(p)}\end{pmatrix} = \begin{pmatrix}\boldsymbol{r}_{2N+2}^{(p)} & \cdots & \boldsymbol{r}_{4N+2}^{(p)}\end{pmatrix}. \tag{36}$$

Then, when the error is negligible for the guided modes, more accurate results are obtained by replacing $\{\eta_n^{(p)}\}_{n=1}^{2N+1}$ and $\{\boldsymbol{r}_n^{(p)}\}_{n=1}^{2N+1}$ in the following ways:

$$\eta_n^{(p)} = -\eta_{n+2N+1}^{(p)} \tag{37}$$

$$\begin{pmatrix}\boldsymbol{r}_1^{(p)} & \cdots & \boldsymbol{r}_{2N+1}^{(p)}\end{pmatrix} = \begin{pmatrix}\boldsymbol{R}_2^{(p)}\\ \boldsymbol{R}_1^{(p)}\end{pmatrix}, \tag{38}$$

where n in Eq. (37) is any integer $1 \le n \le 2N+1$ and Eq. (38) is presented in Ref. (Miyamoto et al., 2003). Then, if we calculate accurately the Floquet-modes corresponding to the values located in the lower half-plane, the other Floquet-modes are obtained by the symmetry property. The normalized propagation constants of the TE polarized Floquet-modes for the same photonic crystal waveguide as in Fig. 3(a), in which the constants corresponding to the modes propagating in the $+z$-direction are obtained by Eq. (37), are shown in Fig. 3(b). This gives the typical distribution of the constants of the Floquet-modes propagating in the photonic crystal waveguides.
The present approach provides sufficiently accurate results in many applications but it has a limitation for highly accurate computation. The spectral radius of the transfer matrix $\boldsymbol{F}^{(p)}$ becomes larger with the increase of the truncation order N, and the computation with very large N may lead to significant errors for not only the evanescent modes propagating in the $+z$-direction but also the guided modes. In such case, using the symmetric property is no longer effective to improve the accuracy. For example, when the double precision computation is applied to the same waveguide as in Figs. 2 and 3, the guided modes cannot be distinguished from the evanescent ones for $N > 68$. This limitation is some relieved if the eigenvalues are computed as the Rayleigh quotients, but the validity is still limited(Watanabe & Yasumoto, 2009).

3. Floquet-Modal Expansion

Since the propagation constants $\{\eta_n^{(p)}\}_{n=1}^{4N+2}$ and the eigenvectors $\{\boldsymbol{r}_n^{(p)}\}_{n=1}^{4N+2}$ are arranged in such a way that $\{\eta_n^{(p)}\}_{n=1}^{2N+1}$ and $\{\boldsymbol{r}_n^{(p)}\}_{n=1}^{2N+1}$ correspond to the Floquet-modes propagating in the $+z$-direction and that $\{\eta_n^{(p)}\}_{n=2N+2}^{4N+2}$ and $\{\boldsymbol{r}_n^{(p)}\}_{n=2N+2}^{4N+2}$ correspond to ones propagating in the $-z$-direction, the amplitudes of the Floquet-modes $\{b_n^{(p)}(z)\}_{n=1}^{2N+1}$ and $\{b_n^{(p)}(z)\}_{n=2N+2}^{4N+2}$ correspond to the modes propagating in the $+z$- and $-z$-directions, respectively. To express clearly, we use the following notations:

$$b_m^{(p,+)}(z) = b_m^{(p)}(z) \tag{39}$$

$$b_m^{(p,-)}(z) = b_{m+2N+1}^{(p)}(z) \tag{40}$$

for $m = 1,\ldots,2N+1$. Then $b_m^{(p,\pm)}(z)$ gives the amplitude of the mth-order Floquet-mode propagating in the $\pm z$-direction. We rewrite the Fourier coefficients of the modal profile functions corresponding to the mth-order Floquet-modes propagating in the $+z$-direction as follows:

$$\begin{pmatrix} \boldsymbol{e}_{y,m} \\ \boldsymbol{h}_{x,m} \end{pmatrix} = \boldsymbol{Q}_s^{(e)} \boldsymbol{r}_m^{(e)} \tag{41}$$

$$\begin{pmatrix} \boldsymbol{h}_{y,m} \\ \boldsymbol{e}_{x,m} \end{pmatrix} = \boldsymbol{Q}_s^{(h)} \boldsymbol{r}_m^{(h)} \tag{42}$$

for $m = 1,\ldots,2N+1$. Considering Eqs. (19), (20), and (38), the coefficients of the modal profile functions corresponding to the mth-order Floquet-modes propagating in the $-z$-direction are given by

$$\begin{pmatrix} \boldsymbol{e}_{y,m} \\ -\boldsymbol{h}_{x,m} \end{pmatrix} = \boldsymbol{Q}_s^{(e)} \boldsymbol{r}_{m+2N+1}^{(e)} \tag{43}$$

$$\begin{pmatrix} \boldsymbol{h}_{y,m} \\ -\boldsymbol{e}_{x,m} \end{pmatrix} = \boldsymbol{Q}_s^{(h)} \boldsymbol{r}_{m+2N+1}^{(h)}. \tag{44}$$

The coefficients at $z = l\,d_z$ for any integer l are expressed as follows:

$$\begin{pmatrix} \boldsymbol{e}_y(l\,d_z) \\ \boldsymbol{h}_x(l\,d_z) \end{pmatrix} = \sum_{m=1}^{2N+1} b_m^{(e,+)}(l\,d_z) \begin{pmatrix} \boldsymbol{e}_{y,m} \\ \boldsymbol{h}_{x,m} \end{pmatrix} + \sum_{m=1}^{2N+1} b_m^{(e,-)}(l\,d_z) \begin{pmatrix} \boldsymbol{e}_{y,m} \\ -\boldsymbol{h}_{x,m} \end{pmatrix} \tag{45}$$

$$\begin{pmatrix} \boldsymbol{h}_y(l\,d_z) \\ \boldsymbol{e}_x(l\,d_z) \end{pmatrix} = \sum_{m=1}^{2N+1} b_m^{(h,+)}(l\,d_z) \begin{pmatrix} \boldsymbol{h}_{y,m} \\ \boldsymbol{e}_{x,m} \end{pmatrix} + \sum_{m=1}^{2N+1} b_m^{(h,-)}(l\,d_z) \begin{pmatrix} \boldsymbol{h}_{y,m} \\ -\boldsymbol{e}_{x,m} \end{pmatrix} \tag{46}$$

from Eqs. (15), (16), and (28). This gives the Floquet-mode expansion representation for the fields at $z = l\,d_z$ in the Fourier space. From Eqs. (30), (31), and (37), the amplitudes $\{b_m^{(p,\pm)}(z)\}_{m=1}^{2N+1}$ have the following dependence:

$$b_m^{(p,\pm)}(l'\,d_z) = b_m^{(p,\pm)}(l\,d_z)\, e^{\pm i(l'-l)\eta_m^{(p)} d_z} \tag{47}$$

for any integers l and l'.
Here, two field distributions $(\boldsymbol{E}_1, \boldsymbol{H}_1)$ and $(\boldsymbol{E}_2, \boldsymbol{H}_2)$ are known to satisfy Lorentz's reciprocal theorem:

$$\nabla \cdot (\boldsymbol{E}_1(x,z) \times \boldsymbol{H}_2(x,z) - \boldsymbol{E}_2(x,z) \times \boldsymbol{H}_1(x,z)) = 0. \tag{48}$$

Integrating over the layer between $z = l\,d_z$ and $z = l'\,d_z$ for any integers l, l' and using the Gauss theorem, we may obtain the following relation:

$$\begin{aligned} &\int_0^w (\boldsymbol{E}_1(x,l\,d_z) \times \boldsymbol{H}_2(x,l\,d_z) - \boldsymbol{E}_2(x,l\,d_z) \times \boldsymbol{H}_1(x,l\,d_z)) \cdot \hat{\boldsymbol{z}}\,dx \\ &\quad - \int_0^w \left(\boldsymbol{E}_1(x,l'\,d_z) \times \boldsymbol{H}_2(x,l'\,d_z) - \boldsymbol{E}_2(x,l'\,d_z) \times \boldsymbol{H}_1(x,l'\,d_z)\right) \cdot \hat{\boldsymbol{z}}\,dx = 0 \end{aligned} \tag{49}$$

where the fields are assumed to satisfy the periodic boundary condition with period w and $\hat{\boldsymbol{z}}$ denotes the unit vector along the positive z-axis. The Cartesian components of the fields are expressed in the Fourier series expansions. Then, Eq. (49) yields

$$\begin{aligned}&\langle \boldsymbol{e}_{1,y}(l\,d_z)|\boldsymbol{h}_{2,x}(l\,d_z)\rangle - \langle \boldsymbol{e}_{2,y}(l\,d_z)|\boldsymbol{h}_{1,x}(l\,d_z)\rangle \\ &\quad - \langle \boldsymbol{e}_{1,y}(l'\,d_z)|\boldsymbol{h}_{2,x}(l'\,d_z)\rangle + \langle \boldsymbol{e}_{2,y}(l'\,d_z)|\boldsymbol{h}_{1,x}(l'\,d_z)\rangle = 0\end{aligned} \tag{50}$$

for the TE-polarization, and

$$\begin{aligned}&\langle \boldsymbol{e}_{1,x}(l\,d_z)|\boldsymbol{h}_{2,y}(l\,d_z)\rangle - \langle \boldsymbol{e}_{2,x}(l\,d_z)|\boldsymbol{h}_{1,y}(l\,d_z)\rangle \\ &\quad - \langle \boldsymbol{e}_{1,x}(l'\,d_z)|\boldsymbol{h}_{2,y}(l'\,d_z)\rangle + \langle \boldsymbol{e}_{2,x}(l'\,d_z)|\boldsymbol{h}_{1,y}(l'\,d_z)\rangle = 0\end{aligned} \tag{51}$$

for the TM-polarization. For example, $\boldsymbol{e}_{1,y}(z)$ denotes the column matrix of the Fourier coefficients corresponding to the y-component of $\boldsymbol{E}_1(x,z)$. Also, the angle brackets denote an inner product defined by

$$\langle \boldsymbol{a}|\boldsymbol{b}\rangle \equiv \sum_{n=1}^{2N+1} (\boldsymbol{a})_n\,(\boldsymbol{b})_{-n+2N+2} \tag{52}$$

where $\boldsymbol{a}$ and $\boldsymbol{b}$ are vectors of length $2N+1$. Equations (50) and (51) represent Lorentz's reciprocal theorem in the Fourier space.

We choose the mth-order Floquet-mode propagating in the $+z$-direction as the first fields $(\boldsymbol{E}_1, \boldsymbol{H}_1)$ and the m'th-order Floquet-mode propagating in the $\pm z$-direction as the second fields $(\boldsymbol{E}_2, \boldsymbol{H}_2)$. The propagation constants $\eta_m^{(h)}$ and $\eta_{m'}^{(h)}$ are assumed to be equal only when $m = m'$. Then, for the TE-polarization, we use the following column matrices:

$$\begin{pmatrix} \boldsymbol{e}_{1,y}(l\,d_z) \\ \boldsymbol{h}_{1,x}(l\,d_z) \end{pmatrix} = b_m^{(e,+)}(l\,d_z) \begin{pmatrix} \boldsymbol{e}_{y,m} \\ \boldsymbol{h}_{x,m} \end{pmatrix} \tag{53}$$

$$\begin{pmatrix} \boldsymbol{e}_{2,y}(l\,d_z) \\ \boldsymbol{h}_{2,x}(l\,d_z) \end{pmatrix} = b_{m'}^{(e,\pm)}(l\,d_z) \begin{pmatrix} \boldsymbol{e}_{y,m'} \\ \pm\boldsymbol{h}_{x,m'} \end{pmatrix} \tag{54}$$

for any integer l. Substituting into Eq. (50) and using Eq. (47), we obtain

$$\left[1 - e^{i(l'-l)\left(\eta_m^{(e)} \pm \eta_{m'}^{(e)}\right)d_z}\right] \left(\langle \boldsymbol{e}_{y,m}|\boldsymbol{h}_{x,m'}\rangle \mp \langle \boldsymbol{e}_{y,m'}|\boldsymbol{h}_{x,m}\rangle\right) = 0. \tag{55}$$

This relation should hold for any integers l and l'. Since $\eta_m^{(h)} + \eta_{m'}^{(h)} \neq n\,k_d$ for any integer n, we have

$$\langle \boldsymbol{e}_{y,m}|\boldsymbol{h}_{x,m'}\rangle = \langle \boldsymbol{e}_{y,m'}|\boldsymbol{h}_{x,m}\rangle. \tag{56}$$

Also, since $\eta_m^{(h)} - \eta_{m'}^{(h)} = n\,k_d$ for any integer n only when $m = m'$, we derive the following relation:

$$\langle \boldsymbol{e}_{y,m}|\boldsymbol{h}_{x,m'}\rangle = \delta_{m,m'}\,\langle \boldsymbol{e}_{y,m}|\boldsymbol{h}_{x,m}\rangle. \tag{57}$$

Following the similar process, the relation for the TM-polarization is derived as

$$\langle \boldsymbol{e}_{x,m}|\boldsymbol{h}_{y,m'}\rangle = \delta_{m,m'}\,\langle \boldsymbol{e}_{x,m}|\boldsymbol{h}_{y,m}\rangle. \tag{58}$$

Equations (57) and (58) represent the orthogonal relations of the Floquet-modes.
As mentioned before, the coefficient matrices of the fields at $z = l\,d_z$ for any integer l are expressed by Eqs. (45) and (46). Calculating $\langle \boldsymbol{e}_y(l\,d_z)|\boldsymbol{h}_{x,m'}\rangle \pm \langle \boldsymbol{e}_{y,m'}|\boldsymbol{h}_x(l\,d_z)\rangle$ and $\langle \boldsymbol{e}_x(l\,d_z)|\boldsymbol{h}_{y,m'}\rangle \pm \langle \boldsymbol{e}_{x,m'}|\boldsymbol{h}_y(l\,d_z)\rangle$ for the TE- and the TM-polarizations, respectively, the orthogonal relations (57) and (58) yield the amplitudes of the Floquet-modes as

$$b_m^{(e,\pm)}(l\,d_z) = \frac{\langle \boldsymbol{e}_y(l\,d_z)|\boldsymbol{h}_{x,m}\rangle \pm \langle \boldsymbol{e}_{y,m}|\boldsymbol{h}_x(l\,d_z)\rangle}{2\,\langle \boldsymbol{e}_{y,m}|\boldsymbol{h}_{x,m}\rangle} \tag{59}$$

for the TE-polarization, and

$$b_m^{(h,\pm)}(l\,d_z) = \frac{\pm\langle \boldsymbol{e}_x(l\,d_z)|\boldsymbol{h}_{y,m}\rangle + \langle \boldsymbol{e}_{x,m}|\boldsymbol{h}_y(l\,d_z)\rangle}{2\,\langle \boldsymbol{e}_{x,m}|\boldsymbol{h}_{y,m}\rangle} \tag{60}$$

for the TM-polarization.

4. Discontinuities in Photonic Crystal Waveguides

Next, we consider nonuniform structures formed by defects in a photonic crystal as shown in Fig. 4. The fields are assumed to be well confined in $0 < x < w$ and approximated by periodic functions of x with the period w as same with in the previous sections. The structure is decomposed into three sections. The regions $z < 0$ and $z > h$ ($h = L\,d_z$) are input/output waveguide sections consisting of the straight line defects, while the region $0 < z < h$ is a transition section where the periodicity breaks. The structure is considered as a series of step-transitions of the photonic crystal waveguides and we apply the S-matrix propagation algorithm(Li, 1996a).
For $p = e,h$, the matrices $\boldsymbol{R}^{(p)}$ given by Eq. (29) and the Floquet-modal amplitudes $\{b_m^{(p,\pm)}(z)\}_{m=1}^{2N+1}$ given by Eqs. (39), (40) for the regions $(l-1)\,d_z < z < l\,d_z$ ($l = 0,\ldots,L+1$) are denoted by $\boldsymbol{R}^{(p,l)}$ and $\{b_m^{(p,l,\pm)}(z)\}_{m=1}^{2N+1}$, respectively. Also, we use the column matrix $\boldsymbol{b}^{(p,l,\pm)}(z)$ whose mth-component is $b_m^{(p,l,\pm)}(z)$. Considering $\boldsymbol{b}^{(p,l,\pm)}(z)$ gives the amplitudes

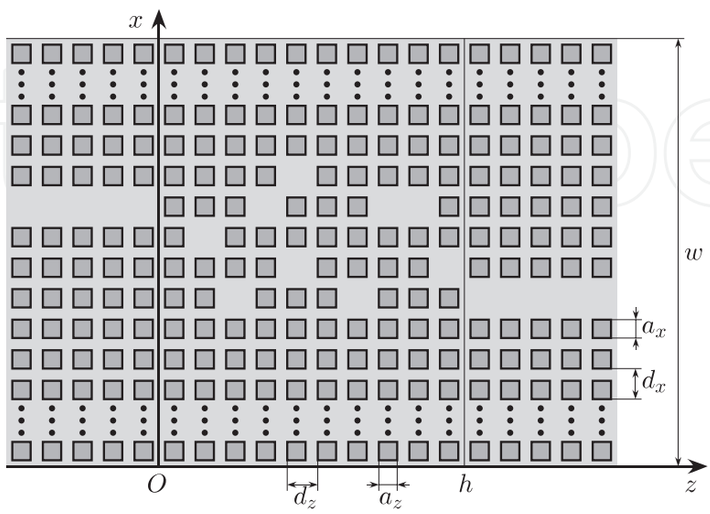

Fig. 4. Nonuniform structure formed by defects in photonic crystal.

of the Floquet-modes propagating in the $\pm z$-direction, the S-matrix of the region $0 < z < l\,d_z$ are defined by

$$\begin{pmatrix} \boldsymbol{b}^{(p,0,-)}(0) \\ \boldsymbol{b}^{(p,l+1,+)}(l\,d_z) \end{pmatrix} = \begin{pmatrix} \boldsymbol{S}_{l,11}^{(p)} & \boldsymbol{S}_{l,12}^{(p)} \\ \boldsymbol{S}_{l,21}^{(p)} & \boldsymbol{S}_{l,22}^{(p)} \end{pmatrix} \begin{pmatrix} \boldsymbol{b}^{(p,0,+)}(0) \\ \boldsymbol{b}^{(p,l+1,-)}(l\,d_z) \end{pmatrix} \tag{61}$$

where $\boldsymbol{S}_{l,11}^{(p)}$, $\boldsymbol{S}_{l,12}^{(p)}$, $\boldsymbol{S}_{l,21}^{(p)}$, and $\boldsymbol{S}_{l,22}^{(p)}$ are $(2N+1) \times (2N+1)$ square submatrices. The boundary condition at $z = l\,d_z$ $(l = 0, \ldots, L)$ is matched by equating the Fourier coefficients of tangential field components in both sides of the step-transition, and yields

$$\begin{pmatrix} \boldsymbol{b}^{(p,l+1,+)}(l\,d_z) \\ \boldsymbol{b}^{(p,l+1,-)}(l\,d_z) \end{pmatrix} = \begin{pmatrix} \boldsymbol{G}_{11}^{(p,l)} & \boldsymbol{G}_{12}^{(p,l)} \\ \boldsymbol{G}_{21}^{(p,l)} & \boldsymbol{G}_{22}^{(p,l)} \end{pmatrix} \begin{pmatrix} \boldsymbol{b}^{(p,l,+)}(l\,d_z) \\ \boldsymbol{b}^{(p,l,-)}(l\,d_z) \end{pmatrix} \tag{62}$$

with

$$\begin{pmatrix} \boldsymbol{G}_{11}^{(p,l)} & \boldsymbol{G}_{12}^{(p,l)} \\ \boldsymbol{G}_{21}^{(p,l)} & \boldsymbol{G}_{22}^{(p,l)} \end{pmatrix} = {\boldsymbol{R}^{(p,l+1)}}^{-1}\,\boldsymbol{R}^{(p,l)}. \tag{63}$$

From Eq. (62) for $l = 0$, the initial S-matrices are derived as follows:

$$\boldsymbol{S}_{0,12}^{(p)} = {\boldsymbol{G}_{22}^{(p,0)}}^{-1} \tag{64}$$

$$\boldsymbol{S}_{0,11}^{(p)} = -\boldsymbol{S}_{0,12}^{(p)}\,\boldsymbol{G}_{21}^{(p,0)} \tag{65}$$

$$\boldsymbol{S}_{0,21}^{(p)} = \boldsymbol{G}_{11}^{(p,0)} + \boldsymbol{G}_{12}^{(p,0)}\,\boldsymbol{S}_{0,11}^{(p)} \tag{66}$$

$$\boldsymbol{S}_{0,22}^{(p)} = \boldsymbol{G}_{12}^{(p,0)}\,\boldsymbol{S}_{0,12}^{(p)}. \tag{67}$$

Also, Eq. (47) gives the following relations:

$$\boldsymbol{b}^{(p,l,+)}(l\,d_z) = \boldsymbol{D}^{(p,l)}\,\boldsymbol{b}^{(p,l,+)}((l-1)\,d_z) \tag{68}$$

$$\boldsymbol{b}^{(p,l,-)}((l-1)\,d_z) = \boldsymbol{D}^{(p,l)}\,\boldsymbol{b}^{(p,l,-)}(l\,d_z) \tag{69}$$

$$\left(\boldsymbol{D}^{(p,l)}\right)_{n,m} = \delta_{n,m}\,e^{i\,\eta_m^{(p,l)}\,d_z} \tag{70}$$

for $1, \ldots, L$, where $\{\eta_m^{(p,l)}\}_{m=1}^{2N+1}$ are the propagation constants of the Floquet-modes in each region $(l-1)\,d_z < z < l\,d_z$. When the S-matrices $\boldsymbol{S}_{l-1,11}^{(p)}$, $\boldsymbol{S}_{l-1,12}^{(p)}$, $\boldsymbol{S}_{l-1,21}^{(p)}$, and $\boldsymbol{S}_{l-1,22}^{(p)}$ are given, the S-matrices $\boldsymbol{S}_{l,11}^{(p)}$, $\boldsymbol{S}_{l,12}^{(p)}$, $\boldsymbol{S}_{l,21}^{(p)}$, and $\boldsymbol{S}_{l,22}^{(p)}$ are derived from Eqs. (61), (62), (68), and (69) as follows:

$$\boldsymbol{S}_{l,12}^{(p)} = \boldsymbol{S}_{l-1,12}^{(p)}\,\boldsymbol{D}^{(p,l)}\,{\boldsymbol{W}_{l,1}^{(p)}}^{-1} \tag{71}$$

$$\boldsymbol{S}_{l,11}^{(p)} = \boldsymbol{S}_{l-1,11}^{(p)} - \boldsymbol{S}_{l,12}^{(p)}\,\boldsymbol{G}_{21}^{(p,l)}\,\boldsymbol{D}^{(p,l)}\,\boldsymbol{S}_{l-1,21}^{(p)} \tag{72}$$

$$\boldsymbol{S}_{l,22}^{(p)} = \boldsymbol{W}_{l,2}^{(p)}\,{\boldsymbol{W}_{l,1}^{(p)}}^{-1} \tag{73}$$

$$\boldsymbol{S}_{l,21}^{(p)} = \left(\boldsymbol{G}_{11}^{(p,l)} - \boldsymbol{S}_{l,22}^{(p)}\,\boldsymbol{G}_{21}^{(p,l)}\right)\boldsymbol{D}^{(p,l)}\,\boldsymbol{S}_{l-1,21}^{(p)} \tag{74}$$

with

$$\boldsymbol{W}_{l,1}^{(p)} = \boldsymbol{G}_{22}^{(p,l)} + \boldsymbol{G}_{21}^{(p,l)} \boldsymbol{D}^{(p,l)} \boldsymbol{S}_{l-1,22}^{(p)} \boldsymbol{D}^{(p,l)} \tag{75}$$

$$\boldsymbol{W}_{l,2}^{(p)} = \boldsymbol{G}_{12}^{(p,l)} + \boldsymbol{G}_{11}^{(p,l)} \boldsymbol{D}^{(p,l)} \boldsymbol{S}_{l-1,22}^{(p)} \boldsymbol{D}^{(p,l)}. \tag{76}$$

Consequently, the S-matrices $\boldsymbol{S}_{L,11}^{(p)}$, $\boldsymbol{S}_{L,12}^{(p)}$, $\boldsymbol{S}_{L,21}^{(p)}$, and $\boldsymbol{S}_{L,22}^{(p)}$ for the entire transition section are obtained by the initial matrices (64)–(67) and the recursive relations (71)–(76).

The proposed method has been used to analyze several fundamental photonic crystal circuit components(Yasumoto & Watanabe, 2008a;b). The photonic crystal consists of identical rectangular cylinders situated parallel in rectangular lattice. The permittivities of the surrounding medium and the cylinders are $\varepsilon_s = \varepsilon_0$ and $\varepsilon_c = 12.25\varepsilon_0$. The dimensions of the cylinders are $a_x = a_z = 0.2\sqrt{\pi}\, d_x$ and the lattice constants are $d_x = d_z = 340\,\mu$m. We consider the TE-polarized fields, and the photonic crystal waveguides formed by a straight line defect in the photonic crystal support only one guided Floquet-mode.

First, we consider a directional coupler with the coupling length with $h = 10\, d_z$ as shown in Fig. 5(a). The wavelength in free space and the artificial periodicity for FSEM are chosen as $\lambda_0 = 1\,$mm and $w = 20\, d_x$. The incident wave is the guided Floquet-mode of the uniform waveguide in $z < 0$. If the guided mode is arranged to be the first-order mode, this incident condition is given as

$$b_m^{(e,0,+)}(0) = \delta_{m,1} \tag{77}$$

$$b_m^{(e,L+1,-)}(h) = 0 \tag{78}$$

for $m = 1, \ldots, 2N+1$. Let $\boldsymbol{e}_{y,m}^{(l)}$ and $\boldsymbol{h}_{x,m}^{(l)}$ denote the Fourier coefficient matrices of the modal profile functions corresponding to the mth-order Floquet modes in each region $(l-1)\, d_z < z < l\, d_z$. Then, the transmitted and the reflected powers are respectively calculated by

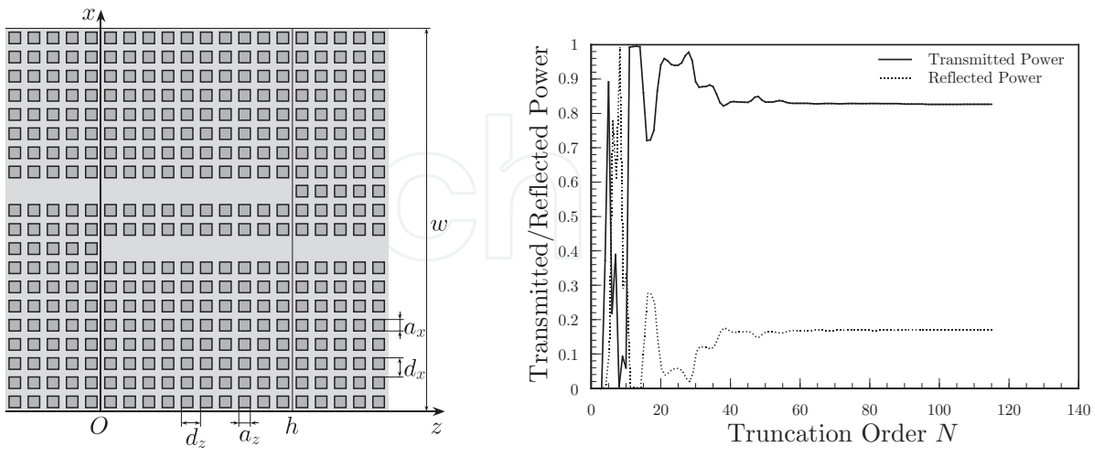

(a) (b)

Fig. 5. Photonic crystal direction couplers: (a) structure under consideration and (b) convergence of the normalized reflection and transmitted powers as functions of the truncation order N.

$(s_1^{(e,L+1)}/s_1^{(e,0)})\,|b_1^{(e,L+1,+)}(h)|^2$ and $|b_1^{(e,0,-)}(0)|^2$ with $s_m^{(e,l)} = -w\Re(\boldsymbol{e}_{y,m}^{(l)} \cdot \boldsymbol{h}_{x,m}^{(l)\,*})/2$, and they are shown in Fig. 5(b) as functions of the truncation order N of the Fourier series expansions. We can see that a good convergence is obtained for $N \gtrsim 4w/d_x$.

Figures 6 and 7 are the results of the photonic crystal waveguide filters. The filters are formed with resonant cavities on the defect layers as shown in Figs. 6(a) and 7(a), and the power transmission and reflection spectra through the resonant cavities are plotted in Figs. 6(b) and 7(b) as functions of the wavelength λ_0. It is seen that the transmission spectra have resonance peaks at around $\lambda_0 = 0.91\,\mathrm{mm}$. Since the resonant cavity in Fig. 7 is weakly coupled with the feed waveguides, its resonance peak is much sharper than that shown in Fig. 6.

The present formulation is also applied to photonic crystal waveguide cranks shown in Figs. 8(a) and 9(a), in which wave propagates perpendicular partially to the z-direction and

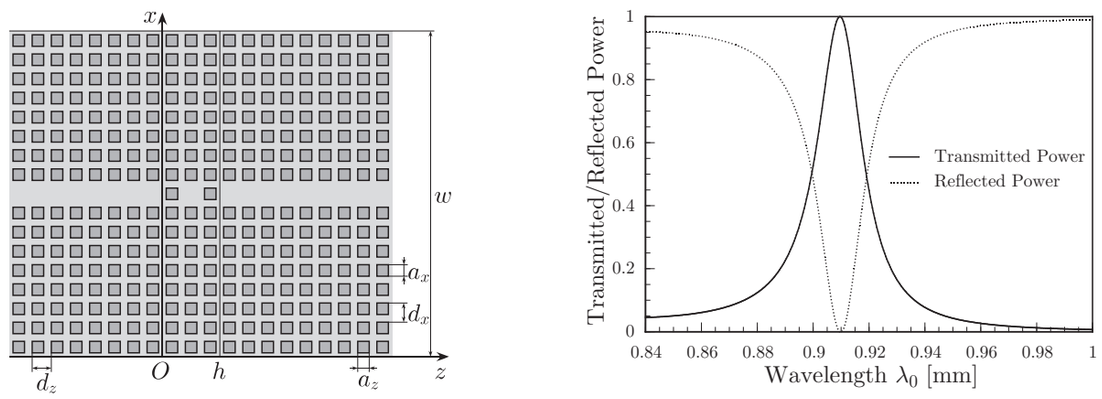

(a) (b)

Fig. 6. Photonic crystal waveguide filter with a resonant cavity strongly coupled to the feed waveguides: (a) structure under consideration and (b) power transmission spectra.

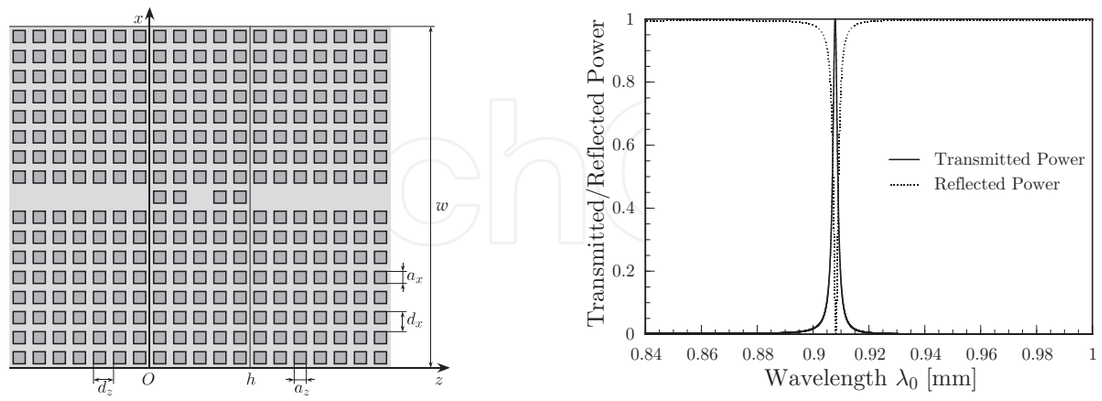

(a) (b)

Fig. 7. Photonic crystal waveguide filter with a resonant cavity weakly coupled to the feed waveguides: (a) structure under consideration and (b) power transmission spectra. (Reproduced from K. Yasumoto and K. Watanabe, *International Journal of Microwave and Optical Technology*, 3, 397–403, 2008, with courtesy of ISRAMT/IJMOT.)

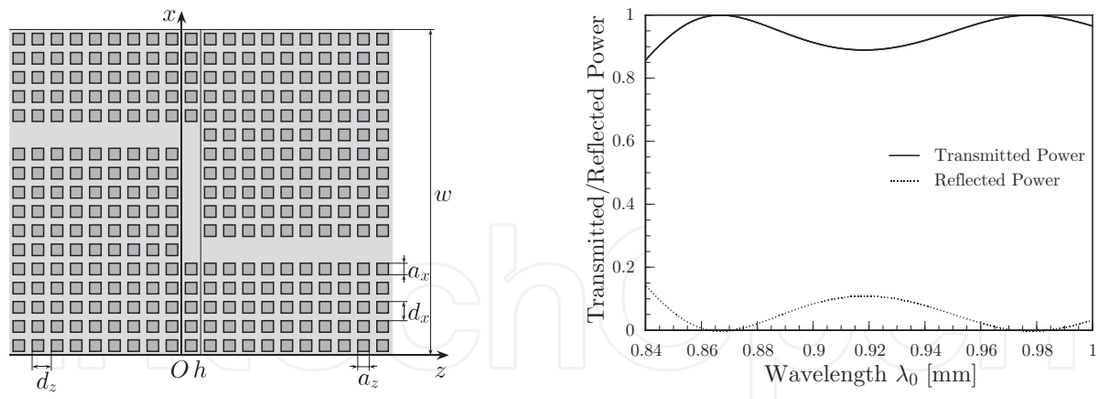

(a) (b)

Fig. 8. Conventional crank of the photonic crystal waveguide: (a) structure under consideration and (b) power transmission spectra. (Reproduced from K. Yasumoto and K. Watanabe, *Proc. of CJMW2008*, 3–8, 2008, with courtesy of IEICE.)

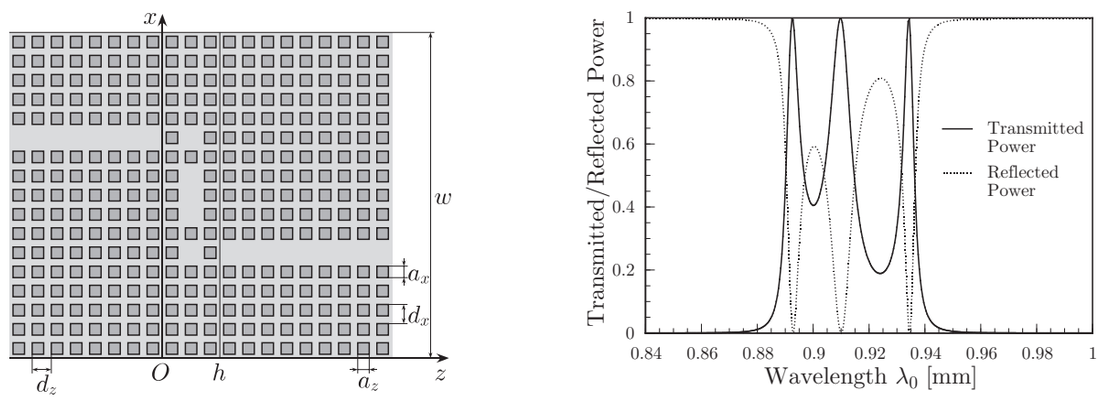

(a) (b)

Fig. 9. Photonic crystal waveguide crank with two resonant cavities: (a) structure under consideration and (b) power transmission spectra. (Reproduced from K. Yasumoto and K. Watanabe, *Proc. of CJMW2008*, 3–8, 2008, with courtesy of IEICE.)

the artificial periodicity is chosen as $w = 17d_x$. The conventional crank has no resonance in the transmission and the reflection spectra as shown in Fig. 8(b). However, when two resonant cavities are introduced in the crank, there appear three resonant peaks in the transmission and the reflection spectra as shown in Fig. 9(b). The center peak corresponds to the resonance wavelength of each isolated cavity (see Fig. 6), whereas other two peaks seem to represent the resonant coupling between two cavities.

Next, we consider the photonic crystal waveguide branches shown in Figs. 10(a), 11(a), and 12(a). The incident wave is the guided Floquet-mode of the uniform waveguide in $z < 0$ and, then, this incident condition is also given by Eqs. (77) and (78). In these structures, the section $z > h$ consists of two parallel waveguides, and we are interested in the transmitted power for each waveguide. Here we denote the upper waveguide by "1" and the lower one

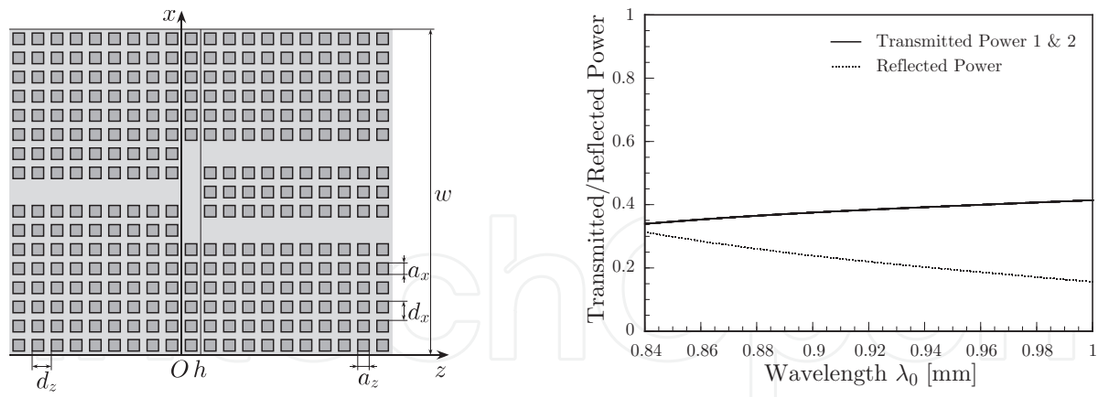

(a) (b)

Fig. 10. Symmetric branch of the photonic crystal waveguide: (a) structure under consideration and (b) power transmission spectra.

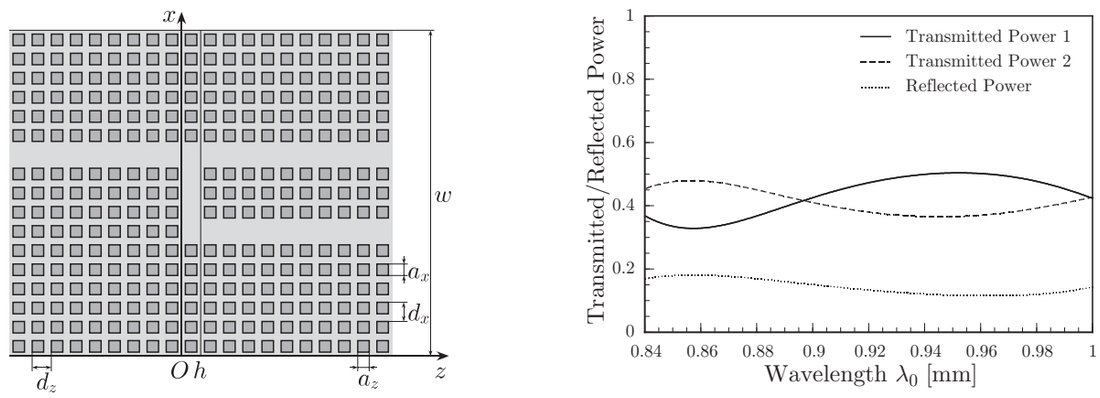

(a) (b)

Fig. 11. Asymmetric branch of the photonic crystal waveguide: (a) structure under consideration and (b) power transmission spectra.

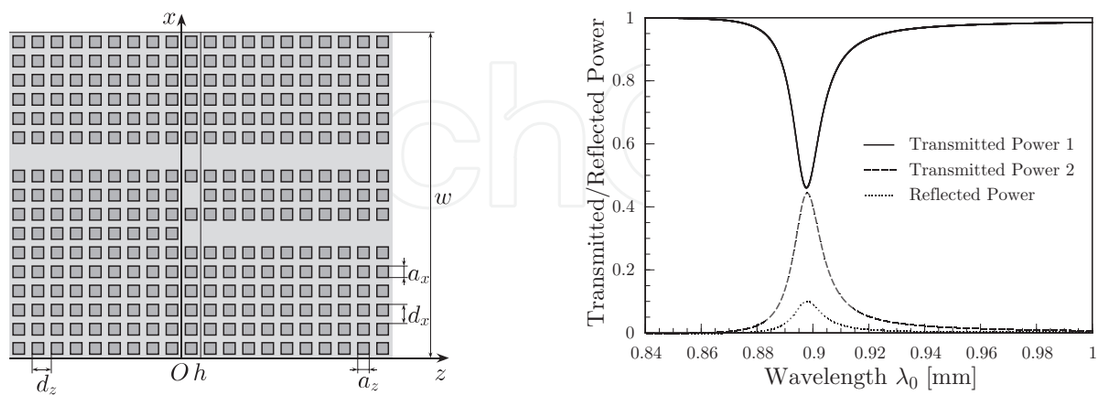

(a) (b)

Fig. 12. Asymmetric branch of the photonic crystal waveguide with a resonant cavity: (a) structure under consideration and (b) power transmission spectra. (Reproduced from K. Yasumoto and K. Watanabe, *Proc. of CJMW2008*, 3–8, 2008, with courtesy of IEICE.)

by "2." Let $\bar{\boldsymbol{e}}_{y,\nu,m}$ and $\pm\bar{\boldsymbol{h}}_{x,\nu,m}$ be the Floquet coefficient matrices of the modal profile functions corresponding to the mth-order Floquet-modes of the isolated waveguides ν ($\nu = 1,2$) propagating in the $\pm z$-direction, and $\bar{b}_{\nu,m}^{(e,l,\pm)}(z)$ be the associated modal amplitudes for the regions $(l-1)\,d_z < z < l\,d_z$ ($l = 0,\ldots,L+1$). From Eqs. (45) and (59), the relation between the amplitudes of the isolated waveguide modes and the compound modes are derived as

$$\bar{b}_{\nu,m}^{(e,l,\pm)}(l'\,d_z) = \sum_{m'=1}^{2N+1} b_{m'}^{(e,l,\pm)}(l'\,d_z)\,\frac{\langle \boldsymbol{e}_{y,m'}^{(l)}|\bar{\boldsymbol{h}}_{x,\nu,m}\rangle + \langle \bar{\boldsymbol{e}}_{y,\nu,m}|\boldsymbol{h}_{x,m'}^{(l)}\rangle}{2\,\langle \bar{\boldsymbol{e}}_{y,\nu,m}|\bar{\boldsymbol{h}}_{x,\nu,m}\rangle} \tag{79}$$

where the counter directional couplings are ignored. If the guided mode is arranged to be the first-order mode, the transmitted powers for the waveguides ν are therefore calculated by $(\bar{s}_{\nu,1}^{(e)}/s_1^{(e,0)})\,|\bar{b}_{\nu,1}^{(e,L+1,+)}(h)|^2$ with $\bar{s}_{\nu,1}^{(e)} = -w\,\Re(\bar{\boldsymbol{e}}_{y,\nu,1}\cdot\bar{\boldsymbol{h}}_{x,\nu,1}^{*})/2$. The transmitted and the reflected powers for the conventional branches are shown in Figs. 10(b), 11(b) as functions of the wavelength. It is seen that the spectra have no sharp resonant peak. On the other hand, Fig. 12(b) shows the spectra for a branch with a resonant cavity. The input power is dropped from the waveguide 1 to the waveguide 2 through the resonance, and almost equally divided into two transmission ports at the resonant wavelength with a small reflection.

The last examples are photonic crystal waveguide couplers with resonant cavities as shown in Figs. 13(a) and 14(a). The incident wave is the guided Floquet-mode of the waveguide 1 in isolation and comes from $z < 0$. If the guided mode is arranged to the first-order mode, the incident condition is given as

$$b_m^{(e,0,+)}(0) = \frac{\langle \bar{\boldsymbol{e}}_{y,1,1}|\boldsymbol{h}_{x,m}^{(0)}\rangle + \langle \boldsymbol{e}_{y,m}^{(0)}|\bar{\boldsymbol{h}}_{x,1,1}\rangle}{2\,\langle \boldsymbol{e}_{y,m}^{(0)}|\boldsymbol{h}_{x,m}^{(0)}\rangle} \tag{80}$$

$$b_m^{(e,L+1,-)}(h) = 0. \tag{81}$$

Then the transmitted and the reflected powers for the isolated waveguides ν are calculated by $(\bar{s}_{\nu,1}^{(e)}/\bar{s}_{1,1}^{(e)})\,|\bar{b}_{\nu,1}^{(e,L+1,+)}(h)|^2$ and $(\bar{s}_{\nu,1}^{(e)}/\bar{s}_{1,1}^{(e)})\,|\bar{b}_{\nu,1}^{(e,0,-)}(0)|^2$, respectively. The transmitted and

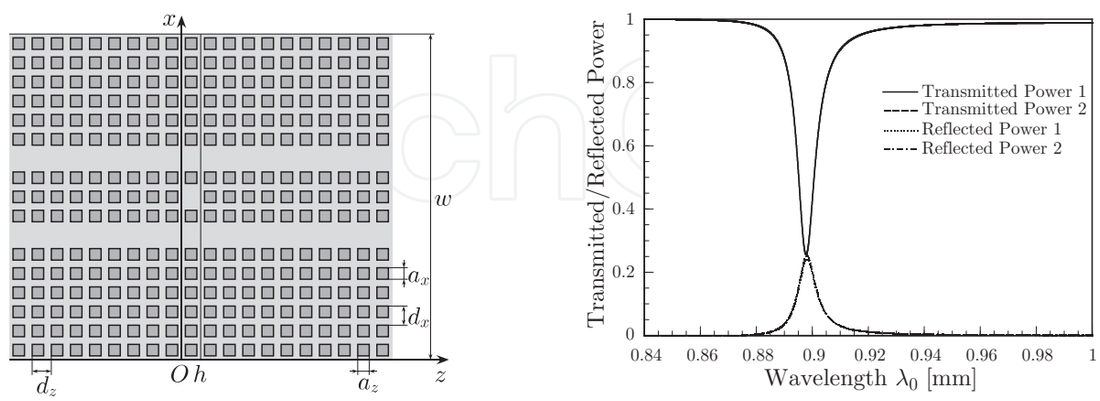

(a) (b)

Fig. 13. Photonic crystal waveguide coupler with a resonant cavity: (a) structure under consideration and (b) power transmission spectra. (Reproduced from K. Yasumoto and K. Watanabe, *Proc. of CJMW2008*, 3–8, 2008, with courtesy of IEICE.)

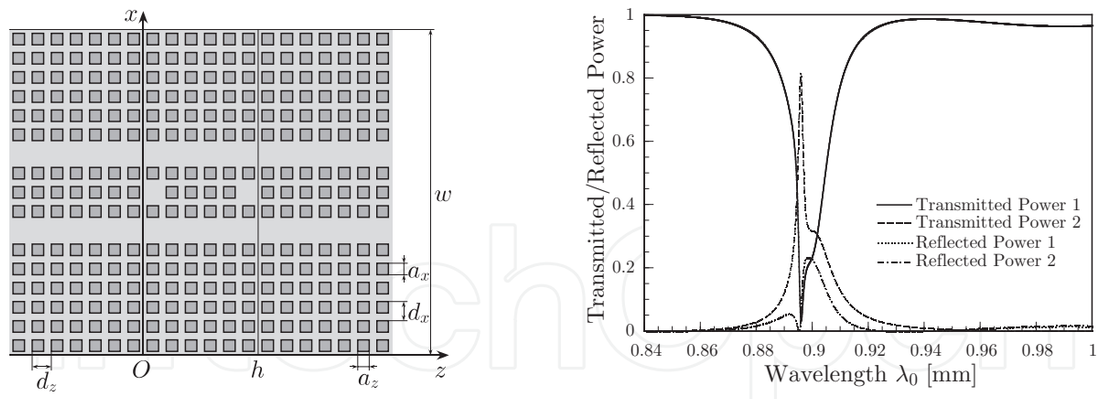

(a) (b)

Fig. 14. Photonic crystal waveguide coupler with two resonant cavities: (a) structure under consideration and (b) power transmission spectra.

the reflected powers for the photonic crystal waveguide coupler with one resonant cavity are shown in Fig. 13(b) as functions of the wavelength. For this configuration, three lines except for the solid lines overlap though it is indiscernible. The input power is equally divided into four output ports at the resonant to the cavity. Figure 14(b) shows the spectra of the coupler with two resonant cavities. Two reflection spectra still overlap but the transmission spectrum of the isolated waveguide 2 separates from them. In this case, about 80 percent of the input power is dropped from the waveguide 1 to the waveguide 2 through the resonance.

5. Conclusion

This chapter has presented the Fourier series expansion method for analyzing the photonic crystal circuit components. The method derives the Floquet-modes by the eigenvalue analysis of the transfer matrix for one periodicity cell in the propagation direction, and the input/output relations are expressed by the S-matrix for the Floquet-modes. The numerical examples for photonic crystal filters, cranks, branches, and couplers have been presented to demonstrate the effectiveness of the present method. We have dealt with the photonic crystals consisting of rectangular cylinders only. However, the method is also applied to the photonic crystals consisting of circular cylinders by introducing the staircase approximation or using a numerical integration to derive the transfer matrix for one periodicity cell. Also, when the number of rows of cylinders on each side of the waveguide is not enough, the radiation loss can be taken into account by introducing the perfectly matched layer near the artificial boundaries(Li & Ho, 2004; Yasumoto et al., 2002; Zhang & Jia, 2007).

Acknowledgments

This work was supported in part by the 2008 grant from the Japan-Indo Collaboration Project on “Infrastructural Communication Technologies Supporting Fully Ubiquitous Information Society.”

6. References

Benisty, H. (1996). Modal analysis of optical guides with two-dimensional photonic band-gap boundaries, *J. Appl. Phys.* **Vol. 79**(No. 10): 7483–7492.

Hosono, T., Hinata, T. & Inoue, A. (1982). Numerical analysis of the discontinuities in slab dielectric waveguides, *Radio Sci.* **Vol. 17**(No. 1): 75–83.

Jia, H. & Yasumoto, K. (2006). Modal analysis of two-dimensional photonic-crystal waveguides formed by rectangular cylinders using an improved fourier series method, *IEEE Trans. Microwave Theory and Techniques* **Vol. 54**(No. 2): 564–571.

Koshiba, M., Tsuji, Y. & Hikari, M. (2000). Time-domain beam propagation method and its application to photonic crystal circuits, *J. Lightwave Technol.* **Vol. 18**(No. 1): 102–110.

Li, L. (1996a). Formulation and comparison of two recursive matrix algorithms for modeling layered diffraction gratings, *J. Opt. Soc. Am. A* **Vol. 13**(No. 5): 1024–1035.

Li, L. (1996b). Use of fourier series in the analysis of discontinuous periodic structures, *J. Opt. Soc. Am. A* **Vol. 13**(No. 9): 1870–1876.

Li, Z. Y. & Ho, K. M. (2003). Light propagation in semi-infinite photonic crystal and related waveguide structures, *Physical Review B* **Vol. 68**: 155101.

Li, Z. Y. & Ho, K. M. (2004). Anomalous propagation loss in photonic crystal waveguides, *Physical Review Lett.* **Vol. 92**(No. 6): 063904.

Miyamoto, T., Momoda, M. & Yasumoto, K. (2003). Numerical analysis for 3-dimensional optical waveguides with periodic structures using fourier series expansion method, *IEICE Trans. Electron.* **Vol. J86-C**(No. 6): 591–600. (in Japanese).

Naka, Y. & Ikuno, H. (2002). Analysis of characteristics of optical waveguide devices constructed by two-dimensional air-hole type photonic crystal, *Proc. Asia-Pacific Eng. Res. Forum on Microwave and Electromagnetic Theory*, pp. 209–218.

Sakoda, K., Ueta, T. & Ohtaka, K. (1997). Numerical analysis of eigenmodes localized at line defects in photonic lattices, *Phys. Rev. B* **Vol. 56**(No. 23): 14905–14908.

Taflove, A. (1995). *Computational Electrodynamics: The Finite-Difference Time-Domain Method*, Artech House, Boston.

Tanaka, H., Yamasaki, T. & Hosono, T. (1994). Propagation characteristics of dielectric waveguides with slanted grating structure, *IEICE Trans. Electron.* **Vol. E77-C**(No. 11): 1820–1827.

Watanabe, K. & Yasumoto, K. (2009). Accuracy improvement of the fourier series expansion method for floquet-mode analysis of photonic crystal waveguides, *Progress In Electromagnetics Res.* **Vol. PIER 92**: 209–222.

Yamakita, J., Matsumoto, K. & Rokushima, K. (1993). Analysis of discontinuities in anisotropic dielectric waveguides, *IEICE Technical Report*. EMT-93-87 (in Japanese).

Yasumoto, K., Jia, H. & Kai, S. (2004). Rigorous analysis of two-dimensional photonic crystal waveguides, *Proc. URSI Int. Symp. on Electromagnetic Theory*, pp. 739–741.

Yasumoto, K., Miyamoto, T. & Momoda, M. (1999). Full-wave analysis of optical waveguides using periodic boundary conditions, *Proc. SPIE* **Vol. 3666**: 170–176.

Yasumoto, K. & Toyama, H. (2001). Formulation for electromagnetic scattering and guidance by two-dimensional photonic crystals, *IEICE Technical Report*. OPE2001-93.

Yasumoto, K. & Watanabe, K. (2008a). Analysis of discontinuities in two-dimensional photonic crystal waveguides using floquet modes concept, *Int. J. Microwave and Opt. Technol.* **Vol. 3**(No. 3): 397–403.

Yasumoto, K. & Watanabe, K. (2008b). Numerical modeling of two-dimensional photonic crystal circuits using fourier modal method based on floquet modes, *Proc. China-Japan Joint Microwave Conf.*, pp. 3–8.

Yasumoto, K., Watanabe, K. & Ishihara, J. (2002). Numerical analysis of optical waveguides with the use of fourier-series expansion method combined with perfectly matched layer, *Microwave Opt. Technol. Lett.* **Vol. 34**(No. 6): 422–426.

Zhang, D. & Jia, H. (2007). Numerical analysis of leaky modes in two-dimensional photonic crystal waveguides using fourier series expansion method with perfectly matched layer, *IEICE Trans. Electron.* **Vol. E90-C**(No. 3): 613–622.

IntechOpen

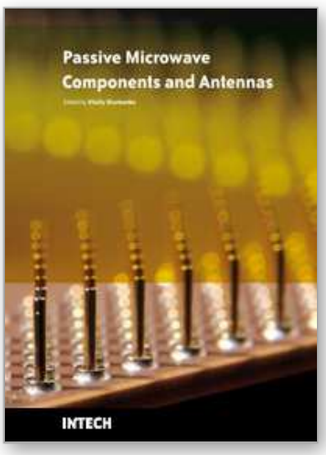

Passive Microwave Components and Antennas

Edited by Vitaliy Zhurbenko

ISBN 978-953-307-083-4
Hard cover, 556 pages
Publisher InTech
Published online 01, April, 2010
Published in print edition April, 2010

Modelling and computations in electromagnetics is a quite fast-growing research area. The recent interest in this field is caused by the increased demand for designing complex microwave components, modeling electromagnetic materials, and rapid increase in computational power for calculation of complex electromagnetic problems. The first part of this book is devoted to the advances in the analysis techniques such as method of moments, finite-difference time- domain method, boundary perturbation theory, Fourier analysis, mode-matching method, and analysis based on circuit theory. These techniques are considered with regard to several challenging technological applications such as those related to electrically large devices, scattering in layered structures, photonic crystals, and artificial materials. The second part of the book deals with waveguides, transmission lines and transitions. This includes microstrip lines (MSL), slot waveguides, substrate integrated waveguides (SIW), vertical transmission lines in multilayer media as well as MSL to SIW and MSL to slot line transitions.

InTech Europe
University Campus STeP Ri
Slavka Krautzeka 83/A
51000 Rijeka, Croatia
Phone: +385 (51) 770 447
Fax: +385 (51) 686 166
www.intechopen.com

InTech China
Unit 405, Office Block, Hotel Equatorial Shanghai
No.65, Yan An Road (West), Shanghai, 200040, China
中国上海市延安西路65号上海国际贵都大饭店办公楼405单元
Phone: +86-21-62489820
Fax: +86-21-62489821

IntechOpen